Computational Simulations using Time-Dependent Ginzburg–Landau Theory for Nb–Ti-like Microstructures

C.W.W. Haddon, A.I. Blair, F. Schoofs, and D.P. Hampshire.

***Abstract*—Simulations based on time-dependent Ginzburg–Landau theory are employed to determine the critical current for a model system which represents a Nb–Ti-like pinning landscape at low drawing strain. The system consists of ellipsoids of normal metal, with dimensions $60\xi \times 3\xi \times 3\xi$, randomly distributed throughout the superconducting bulk with their long axes parallel to the applied current and perpendicular to the field. These preciptates represent the α-Ti elongated precipitates which act as strong pinning centres in Nb–Ti alloys. We present the volume pinning force density as a function of field across the entire range of precipitate volume fractions and find that optimised material in our model system occurs at 32 vol.% ppt., whereas in real materials the optimum occurs at 25 vol.% ppt. The maximum pinning force density in our simulations is slightly higher ($5.4 \times 10^{-3} J_{\mathrm{D}} B_{\mathrm{c2}}$ vs. $17\,\mathrm{GN{\cdot}m^{-3}} = 4.5 \times 10^{-3} J_{\mathrm{D}} B_{\mathrm{c2}}$) and occurs at a lower reduced field ($0.2 B_{\mathrm{c2}}$ vs. $0.5 B_{\mathrm{c2}}$) than in real materials. We conclude that the broad features of Nb–Ti-like systems are captured in our model, but that the details of the precipitate pinning mechanism are not yet included properly.**

***Index Terms*—critical current density, flux pinning, niobium alloys, numerical simulation**

I. Introduction

CRITICAL currents of high-field superconductors are difficult to predict because of the complexity of both the superconductor itself, as well as the underlying microstructure that pins the fluxons. The volume pinning force density, $\boldsymbol{F}_{\mathrm{p}}$, given by $\boldsymbol{J}_{\mathrm{c}} \times \boldsymbol{B}$ where $\boldsymbol{J}_{\mathrm{c}}$ is the critical current density, depends on the nature and distribution of pins in a complicated way. Historically, simple analytic expressions for critical currents have been found by considering systems containing a single type of pin, typically assuming that either the elementary pinning force or the elastic properties of the lattice dominate [1]–[5]. The reason for pinning has long been understood—a normal inclusion pins vortices because there is a reduction in the free energy when the vortex core overlaps the normal region. However, optimised normal metal coated high-field superconductors in technological conductors contain a huge variety of pins (e.g., atomic impurities, normal inclusions, twin planes, and grain boundaries) at densities which can result in a vortex glass or liquid state [6]–[11]. Hence, in material optimised to maximise high-field J_{c}, the fluxon-fluxon spacing is broadly preserved and the pinning results from a disordered flux-line-lattice interacting with a complex microstructure that changes on the scale of a few nanometres.

Pinning can be visualised and quantified using the framework of time-dependent Ginzburg–Landau (TDGL) theory [12] incorporating spatial variation of the parameters in the Ginzburg–Landau (GL) free energy. Since the TDGL equations cannot be solved analytically except for simple pinning systems, a number of computational methods have been developed [13], [14]. Unfortunately the most general solvers are prohibitively expensive for critical current calculations in realistic 3D systems, and so further simplifications are required.

The computational approach used here is based on the work of Sadovskyy et al., who have proposed a massively-parallel solver for the TDGL equations in the very high-κ limit [11] where the magnetic flux density is homogeneous. After choosing a Landau gauge the independent variables are the order parameter and the scalar potential. The huge reduction in simulation time which this approach provides, allows for systematic exploration of a wide range of microstructures. Since all high-field superconducting materials have relatively high-κ, this approach also opens the possibility of comprehensive comparison between computational and experimental J_{c}-data from important high field superconductors used in applications from MRI to fusion. Optimisation of microstructures for maximal J_{c} has been previously studied using this approach. In [15], spherical metallic precipitates with different diameters were considered and the optimal volume fraction was found at a few different fields. Here, we consider different volume fractions for a single precipitate size over the entire magnetic field range. We visualise pinning by microstructures that are typical of alloys such as Nb–Ti, which is the workhorse material for all high-field applications operating at magnetic fields up to 10 T.

In this paper, we calculate critical current density values and provide visualisations of the flux pinning in Nb–Ti-like systems in magnetic fields up to the upper critical field B_{c2}. The pinning from the normal precipitates is simply modelled by decreasing the condensation energy (i.e., α) so that $T > T_{\mathrm{cn}}$ in the normal region, whilst keeping the other GL parameters the same as the bulk superconductor.

Manuscript receipt and acceptance dates will be inserted here. This work is funded by EPSRC grant EP/L01663X/1 that supports the EPSRC Centre for Doctoral Training in the Science and Technology of Fusion Energy.

C.W.W. Haddon and D.P. Hampshire are with Durham University Superconductivity Group, Centre for Material Physics, Department of Physics, Durham University, UK.

A.I. Blair and F. Schoofs are with the Culham Centre for Fusion Energy (CCFE), Culham Science Centre, Abingdon, UK.

Color versions of one or more of the figures in this paper are available online at http://ieeexplore.ieee.org.

Digital Object Identifier will be inserted here upon acceptance.

II. Time-dependent Ginzburg–Landau theory

We use a standard normalisation of the TDGL equations, with lengths in units of the coherence length, ξ [16].

$$-\eta(\partial_t + i\varphi)\psi = -\widetilde{\alpha}\psi + \widetilde{\beta}|\psi|^2\psi + (-i\nabla + \boldsymbol{A})\widetilde{m}^{-1}(-i\nabla + \boldsymbol{A})\psi \tag{1}$$

$$\boldsymbol{J} - \boldsymbol{J}_\mathrm{n} = \widetilde{m}^{-1}\left(\tfrac{i}{2}(\psi^*\nabla\psi - \psi\nabla\psi^*) - |\psi|^2\boldsymbol{A}\right) = \kappa^2 \operatorname{curl}\operatorname{curl}\boldsymbol{A} + \partial_t\boldsymbol{A} + \nabla\varphi \tag{2}$$

where ψ, $\boldsymbol{A}$, and φ denote the normalised order parameter, vector potential, and scalar potential respectively. The timescale ratio η has the value 5.79 in the dirty limit [12], but is set here to 1 since the stationary solutions of interest should not significantly depend on the dynamics of the non-stationary solutions. The symbols with tildes denote the spatially varying GL parameters that characterise the material at each point in the domain. In this work, the normal precipitates are specified by a change in $\widetilde{\alpha}$ (alone) from $+1$ for superconducting material to -1 for normal metal. The parameters $\widetilde{\beta}$ and $\widetilde{m}^{-1}$ are set to 1 throughout the entire material.

III. Simulations in the very high-κ limit

The general approach for producing the computational solutions follows that of Sadovskyy et al. [11] and so only the most important relevant features are outlined below:

A. Boundary conditions and discretisation

In Sadovskyy's very high-κ limit ($\kappa = 27$ for Nb–Ti [17]) the applied field fully penetrates the superconductor and the magnetic field is assumed to be completely uniform. This reduces the degrees of freedom associated with the vector potential, which are expensive to compute in 3D, and yields TDGL equations for the order parameter and scalar potential.

In order to obtain bulk critical current densities which are representative of large systems, surface effects must be eliminated. However, the usual choice of vector potential depends linearly on the y-coordinate, which would lead to a discontinuity in the vector potential and therefore the current density if strict periodic boundary conditions were implemented. To avoid this, we have implemented Sadovskyy's quasiperiodic boundary conditions, where the magnitude of the order parameter is continuous, but there is a discontinuity in the phase (see Fig. 1), the magnitude of which is determined by requiring current continuity normal to the boundary. The large phase gradients in the x-direction at the upper and lower boundaries do not correspond to large screening currents, which would be expected for insulating boundaries, because they are compensated for by the vector potential.

A current applied in the x-direction, $\boldsymbol{J} = J_x\boldsymbol{e}_x$, can result in flux motion in the y-direction, which produces an average electric field in the x-direction. Since the vector potential is taken to be time-independent, there is a net change in the scalar potential across the system in the x-direction. The discontinuity at the boundary is resolved by introducing a gauge transformation which removes the component of φ corresponding to this net field, $-xE_x$, and adds a time dependent phase $K(t)$ to ψ where $\partial_t K = E_x$. The time-evolution of K is therefore driven by the externally applied current.

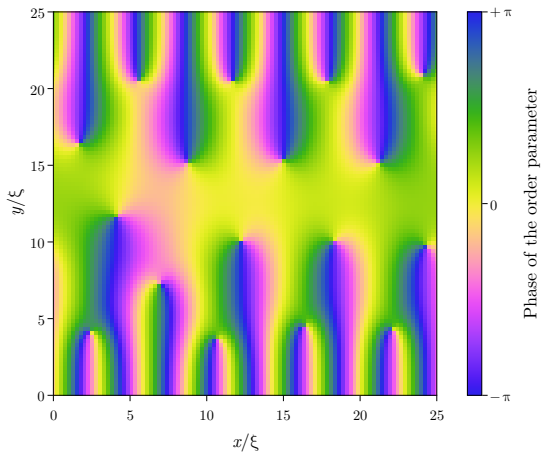

Fig. 1. The phase of the order parameter for a system with quasiperiodic boundary conditions in the y-direction, showing a discontinuity between the upper and lower boundaries. The net field is $0.2B_{\mathrm{c2}}$.

The TDGL equations are then discretised in a modified Crank–Nicolson scheme [18], re-writing the gradient term using link variables to maintain gauge-invariance [13]. The use of an iterative Jacobi method with a maximum norm convergence check results in discrete update equations which can be implemented using local kernel functions, allowing for efficient implementation on a GPU. The equation which describes the evolution of the gauge parameter K, however, depends on the average current, and hence a summation over all grid points is required.

B. Determining the critical current density

A standard search strategy [19] for the critical current density starts with the applied current density at an initial value J_ext which is substantially greater than the critical current [20]. The applied current is then exponentially reduced in steps until J_c is found. For each step, first the current is reduced by 1%, then a time interval is allowed for the transient electric fields which arise from the change in current to dissipate, and then the electric field is averaged over the following time interval. If this average is less than 10^{-5} in normalised units ($4\,\mathrm{V}\cdot\mathrm{m}^{-1}$), it is assumed that the critical current has been reached. Such a large electric field criterion reduces the averaging time required to ensure termination [21] whilst providing sufficiently accurate estimates of the lossless current density.

C. Pinning model

In general the GL parameters for any given superconducting material, α, β, and m (see, e.g., [22, ch. 4]) can be related to a subset of the measurable quantities including: λ (the London penetration depth), ξ, B_{c2}, n_s (the superfluid density), etc. However, most pin types, for example grain boundaries in YBCO, are not superconducting and there are no reliable or

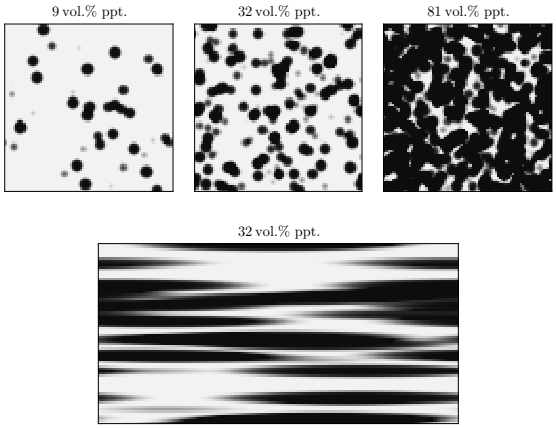

Fig. 2. Transverse cross-sections of $\widetilde{\alpha}(\boldsymbol{r})$ for three different precipitate volume fractions and a single longitudinal cross-section. Black and white represent $\widetilde{\alpha} = -1$ and $\widetilde{\alpha} = +1$ (normal and superconducting) respectively.

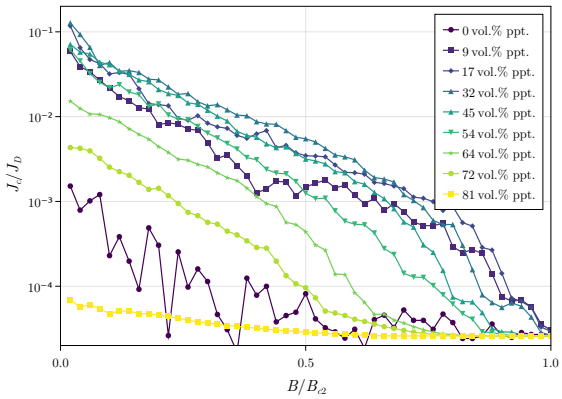

Fig. 3. Critical current data derived from simulations for each precipitate (ppt.) volume fraction. The data for 0 vol.% and 81 vol.% are close to the noise floor for J_c.

precise values known for the GL parameters of the pins in the normal state—not least because the fundamental mechanism that produces superconductivity is still not known, nor is there a detailed microscopic description of the proximity effect [23]. In this paper, we simply implement the pinning with a spatial variation of the relative condensation parameter $\widetilde{\alpha}(\boldsymbol{r}) = \alpha(\boldsymbol{r})/\alpha_s$ where the precipitates are arbitrarily assigned a relative condensation parameter of $\widetilde{\alpha}_n = -1$.

Superconducting alloys can have a wide range of microstructures. Over the course of the wire drawing process for Nb–Ti, the α-Ti precipitates that are the pinning sites, become finer and more closely spaced in the plane perpendicular to the drawing axis [24]. At final strain, they form randomly oriented ribbons of width 1–4 nm with a separation 3–6 nm [24]–[26], less than the fluxon diameter of $2\xi \approx 8\,\mathrm{nm}$. Modelling this optimised microstructure in the TDGL simulation domain is challenging, since a fine grid is required to capture the different length scales of the pinning landscape. Here we have chosen to model a more straightforward system which represents the microstructure at low strain, where the precipitates have been drawn out into simple ellipsoids. Fig. 2 shows transverse cross sections of $\widetilde{\alpha}(\boldsymbol{r})$ for three different precipitate volume fractions in our model, along with a typical longitudinal cross-section. At low volume fractions the ellipsoids are mostly isolated, at intermediate volume fractions several ellipsoids often overlap, and at high volume fractions most of the system is normal and the critical current drops to zero.

In this paper the precipitate diameters in each direction were 60ξ, 3ξ, and 3ξ where the long axis was aligned with the applied current. The procedure for building the material with N precipitates was as follows. First the mesh (dimensions $80\xi \times 40\xi \times 40\xi$) was initialised with $\widetilde{\alpha} = 1$ at all points. Then N precipitates were distributed randomly throughout the simulation domain, accounting for the periodic boundary conditions [27]. Finally the precipitate volume fraction was calculated, which is less than N times the precipitate volume since some precipitates overlap.

IV. Results

The simulated $J_c(B)$ data for systems with different precipitate volume fractions are shown in Fig. 3. The equivalent volume pinning force densities are shown in Figs. 4 and 5. They have been fitted using the pinning function

$$F_p = Ab^p(1-b)^q \tag{3}$$

where $b = B/B_{c2}$ is the reduced field and A, p, and q are fit parameters [3]. We attribute the substantial variations in the critical current data with field for low volume fractions (particularly 9% and 17%), to the many metastable states that occur when the average precipitate spacing is large compared to the system dimensions. As expected, as the volume fraction is increased from zero, there is an increase in the critical current over most of the field range consistent with the linear increase in critical current density with volume fraction observed experimentally in the range 3%–25% [24]. The low volume fractions have relatively high J_c in very high fields (Figs. 3 and 4). At the optimum composition of 32 vol.% ppt., the exponents $p = 0.54$, $q = 2.4$ in our simulations are close to $p = \frac{1}{2}$, $q = 2$, which are usually considered to be representative of surface pinning (e.g., grain boundaries in Nb_3Sn). We note that the maximum pinning force observed was $5.4 \times 10^{-3} J_D B_{c2}$, occurring at $B = 0.2B_{c2}$. For high volume fractions, the exponent q takes values between 3 and 5, which is often attributed to inhomogeneities in the superconducting matrix material because such large values are not found amongst the elementary pinning functions of Dew-Hughes [3], but cannot be the explanation here. This work suggests the relatively large q values may be associated with the proximity effect operating [23] in the vicinity of the normal precipitate pinning sites. For the system with 81 vol.% ppt. the critical current is effectively zero over the entire field range because there is no contiguous superconducting path through the system (Fig. 6).

The model most closely resembles the microstructure found at low drawing strain in the Nb–Ti processing procedure where the precipitates are more ellipsoidal, rather than the high aspect ratio α-Ti ribbons found at higher strains. The

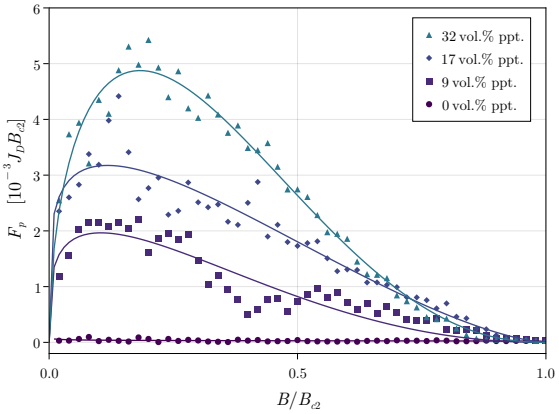

Fig. 4. Pinning force as a function of field for increasing volume percent of precipitates ($\leq$ 32%). The pinning force increases systematically with increasing volume fraction over the entire field range. The lines are fits of the pinning function, Eq. 3.

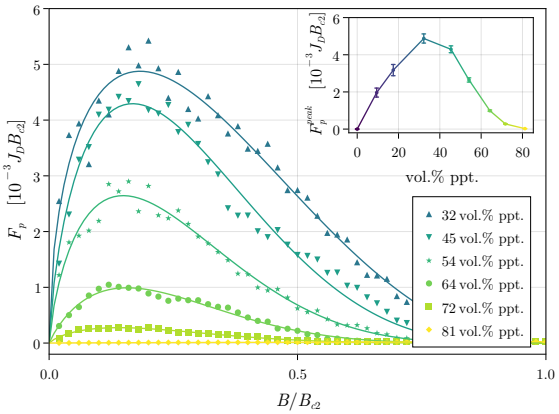

Fig. 5. Pinning force as a function of field for increasing volume percent of precipitates ($\geq$ 32%). The pinning force decreases systematically with increasing volume fraction over the entire field range. The lines are fits of the pinning function, Eq. 3. Inset: peak pinning force versus volume percent of precipitates. Error bars indicate RMS deviation of the data from the pinning curve.

change in the pinning force over the course of the drawing process is complex—the peak in the pinning force density increases in magnitude and moves to higher reduced fields [24]. Comparing our simulations at optimum composition, with the experimental J_c data at 4.2 K from optimised technological conductors, real materials reach a maximum volume pinning force at roughly 25 vol.% ppt., whereas the optimum found in our model is 32 vol.% ppt. The pinning force in state-of-the-art conductors Nb–Ti conductors scales with temperature and strain [29], with the maximum occurring at $B = 0.5B_{c2}$. At 4.2 K, $B_{c2} = 11$ T and the maximum pinning force density is approximately $F_p^{max} = 17\,\mathrm{GN{\cdot}m^{-3}}$ [24], which gives an equivalent dimensionless pinning force density in the best materials of $F_p^{max}/J_D B_{c2} = 4.8 \times 10^{-3}$ (given the zero-field depairing current density, J_D, at 4.2 K is $3.22 \times 10^{11}\,\mathrm{A{\cdot}m^{-2}}$ [30]). This result is similar to the maximum pinning force value found in our simulations of $F_p^{max}/J_D B_{c2} = 5.4 \times 10^{-3}$. We are not aware of other reports of simulations of Nb–Ti-like microstructures, but it is interesting to note that optimal volume fractions of $\sim$23%, similar to those reported here, have been reported in simulations for spherical metallic nanoparticles in an anistotropic superconductor [15].

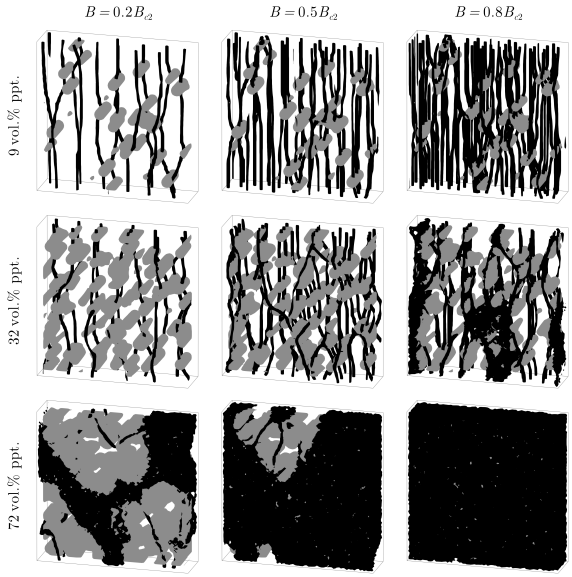

Fig. 6. Snapshots of the vortex matter at three fields for three representative precipitate volume fractions (low, optimised and high). The vortices are visualised in black as the volumes where the squared magnitude of the gauge-invariant phase gradient in the y–z plane exceeds $5/2\xi^2$. Normal regions are therefore entirely black. The precipitates are indicated in grey and have been cut away near the surface to improve visibility. An animated version of this figure is available online [28].

V. Conclusions and Future Work

We have presented TDGL simulations for Nb–Ti-like superconductors with promising results—the field dependence and magnitude of J_c, as well as the optimum volume fraction of normal precipitates are similar to those found in state-of-the-art Nb–Ti materials. We attribute the differences between our simulations and experimental data predominantly to the simple description of the pinning sites we have used in the model, including their ellipsoidal shape and the relatively arbitrary choice $\widetilde{\alpha}_n = -1$ [19]. In future work, we will implement a more realistic description of the pinning sites including both the δH_c pinning and the $\delta\kappa$ pinning that are expected to operate in Nb–Ti [31] (implemented by developing the code to include the spatial variation of the non-linearity parameter, β). We will also implement a more realistic geometry, orientation, and distribution of the precipitates which will enable more complex flux movement, for example flux flow along the length of the precipitates.

Acknowledgment

This work is funded by EPSRC grant EP/L01663X/1 and the UK Government Department for Business, Energy & Industrial Strategy. Data are available at https://doi.org/10.15128/r2tm70mv249 and associated materials can be found at https://dro.dur.ac.uk. The code for the simulations here is available on request from D.P. Hampshire.

REFERENCES

[1] A. M. Campbell and J. E. Evetts, "Flux vortices and transport currents in type II superconductors," *Advances in Physics*, vol. 21, no. 90, pp. 395–399, 1972.

[2] E. J. Kramer, "Scaling laws for flux pinning in hard superconductors," *Journal of Applied Physics*, vol. 44, no. 3, pp. 1360–1370, 1973.

[3] D. Dew-Hughes, "Flux pinning mechanisms in type II superconductors," *The Philosophical Magazine: A Journal of Theoretical Experimental and Applied Physics*, vol. 30, no. 2, pp. 293–305, 1974.

[4] A. I. Larkin and Y. N. Ovchinnikov, "Pinning in type II superconductors," *Journal of Low Temperature Physics*, vol. 34, pp. 409–428, 1979.

[5] J. E. Evetts and C. J. G. Plummer, "Flux pinning in polycrystalline A15 bronze route filaments," in *Proc. Int. Symp. on Flux Pinning and Electromagn. Properties of Supercond*, 1985, pp. 146–151.

[6] M. Machida and H. Kaburaki, "Direct simulation of the time-dependant Ginzburg–Landau equation for type-II superconducting thin film: Vortex dynamics and V–I characteristics," *Physical Review Letters*, vol. 71, no. 19, pp. 3206–3209, 1993.

[7] G. Blatter, M. V. Feigel'man, V. B. Geshkenbein, A. I. Larkin, and V. M. Vinokur, "Vortices in high-temperature superconductors," *Reviews of Modern Physics*, vol. 66, no. 4, pp. 1125–1388, 1994.

[8] E. H. Brandt, "The flux-line lattice in superconductors," *Reports on Progress in Physics*, vol. 58, pp. 1465–1594, 1995.

[9] G. J. Carty, M. Machida, and D. P. Hampshire, "Numerical studies on the effect of normal metal coatings on the magnetisation characteristics of type-II superconductors," *Physical Review B*, vol. 71, p. 144507, 2005.

[10] G. J. Carty and D. P. Hampshire, "Visualising the mechanism that determines the critical current density in polycrystalline superconductors using time-dependent Ginzburg–Landau theory," *Physical Review B*, vol. 77, p. 172501, 2008.

[11] I. A. Sadovskyy, A. E. Koshelev, C. L. Phillips, D. A. Karpeyev, and A. Glatz, "Stable large-scale solver for Ginzburg–Landau equations for superconductors," *Journal of Computational Physics*, vol. 294, pp. 639–654, 2015.

[12] A. Schmid, "A time dependent Ginzburg–Landau equation and its application to the problem of resistivity in the mixed state," *Physik der Kondensierten Materie*, vol. 5, no. 4, pp. 302–317, 1966.

[13] W. D. Gropp, H. G. Kaper, G. K. Leaf, D. M. Levine, M. Palumbo, and V. M. Vinokur, "Numerical simulation of vortex dynamics in type-II superconductors," *Journal of Computational Physics*, vol. 123, no. 2, pp. 254–266, 1996.

[14] T. Winiecki and C. S. Adams, "A fast semi-implicit finite difference method for the TDGL equations," *Journal of Computational Physics*, vol. 179, pp. 127–139, 2002.

[15] A. E. Koshelev, I. A. Sadovskyy, C. L. Phillips, and A. Glatz, "Optimization of vortex pinning by nanoparticles using simulations of the time-dependent Ginzburg–Landau model," *Physical Review B*, vol. 93, no. 6, p. 060508, 2016.

[16] A. I. Blair and D. P. Hampshire, "Time-dependent Ginzburg–Landau simulations of the critical current in superconducting films and junctions in magnetic fields," *IEEE Transactions on Applied Superconductivity*, vol. 28, no. 4, pp. 1–5, 2018.

[17] D. P. Hampshire, "A barrier to increasing the critical current density of bulk untextured polycrystalline superconductors in high magnetic fields," *Physica C: Superconductivity*, vol. 296, no. 1, pp. 153–166, 1998.

[18] J. Crank and P. Nicolson, "A practical method for numerical evaluation of solutions of partial differential equations of the heat-conduction type," *Mathematical Proceedings of the Cambridge Philosophical Society*, vol. 43, no. 1, pp. 50–67, 1947.

[19] I. A. Sadovskyy, Y. Jia, M. Leroux, J. Kwon, H. Hu, L. Fang, C. Chaparro, S. Zhu, U. Welp, J.-M. Zuo, Y. Zhang, R. Nakasaki, V. Selvamanickam, G. W. Crabtree, A. E. Koshelev, A. Glatz, and W.-K. Kwok, "Toward superconducting critical current by design," *Advanced Materials*, vol. 28, no. 23, pp. 4593–4600, 2016.

[20] A. I. Blair and D. P. Hampshire, "The critical current density of S–N–S Josephson junctions and polycrystalline superconductors in high magnetic fields," submitted to Los Alamos archive arXiv.org e-Print archive.

[21] I. A. Sadovskyy, A. E. Koshelev, A. Glatz, V. Ortalan, M. W. Rupich, and M. Leroux, "Simulation of the vortex dynamics in a real pinning landscape of $yba_2cu_3o_{7-\delta}$ coated conductors," *Physical Review Applied*, vol. 5, p. 014011, 2016.

[22] M. Tinkham, *Introduction to Superconductivity*, 2nd ed., ser. Dover Books on Physics. Dover, 2004.

[23] P. G. De Gennes and J. P. Hurault, "Proximity effects under magnetic fields II," *Phys. Lett.*, vol. 17, no. 3, pp. 181–182, 1965.

[24] P. J. Lee, "Abridged metallurgy of ductile alloy superconductors," *Wiley Encyclopedia of Electrical and Electronics Engineering*, vol. 21, pp. 75–87, 1999.

[25] P. Lee and D. Larbalestier, "Development of nanometer scale structures in composites of NbTi and their effect on the superconducting critical current density," *Acta Metallurgica*, vol. 35, no. 10, pp. 2523–2536, 1987.

[26] C. Meingast, P. J. Lee, and D. C. Larbalestier, "Quantitative description of a high J_c Nb–Ti superconductor during its final optimization strain. I. microstructure, T_c, H_{c2}, and resistivity," *Journal of Applied Physics*, vol. 66, no. 12, pp. 5962–5970, 1989.

[27] A. I. Blair and D. P. Hampshire, "Modeling the critical current of polycrystalline superconducting films in high magnetic fields," *IEEE Transactions on Applied Superconductivity*, vol. 29, no. 5, pp. 1–5, 2019.

[28] "Flux pinning in Nb–Ti-like superconductors by ellipsoidal precipitates," 2021. [Online]. Available: https://youtu.be/7KmiTSx_Rok

[29] S. B. L. Chislett-McDonald, Y. Tsui, E. Surrey, M. Kovari, and D. P. Hampshire, "The magnetic field, temperature, strain and angular dependence of the critical current density for Nb–Ti," *Journal of Physics: Conference Series*, vol. 1559, p. 012063, 2020.

[30] G. Wang, M. J. Raine, and D. P. Hampshire, "How resistive must grain boundaries in polycrystalline superconductors be, to limit J_c?" *Superconductor Science and Technology*, vol. 30, no. 10, p. 104001, Aug 2017.

[31] C. Meingast and D. C. Larbalestier, "Quantitative description of a very high critical current density Nb–Ti superconductor during its final optimization strain. II. flux pinning mechanisms," *Journal of Applied Physics*, vol. 66, no. 12, pp. 5971–5983, 1989.